A high-order discontinuous Galerkin approximation to ordinary differential equations with applications to elastodynamics

P.F. ANTONIETTI[1], N. DAL SANTO[2], I. MAZZIERI[1], A. QUARTERONI[2,3]

July 28, 2016

[1] MOX, Dipartmento di Matematica, Politecnico di Milano,
Piazza Leonardo da Vinci 32, 20133 Milano, Italy
paola.antonietti@polimi.it,ilario.mazzieri@polimi.it

[2] CMCS, École Polytechnique Fédérale de Lausanne (EPFL),
Station 8, 1015 Lausanne, Switzerland.
alfio.quarteroni@epfl.ch, niccolo.dalsanto@epfl.ch

[3] MOX, Dipartmento di Matematica, Politecnico di Milano,
Piazza Leonardo da Vinci 32, 20133 Milano, Italy (on leave)

Keywords: space-time finite elements, discontinuous Galerkin methods, second order hyperbolic equations.

AMS Subject Classification: 65M55, 65M70, 35Q86.

Abstract

The aim of this work is to propose and analyze a new high order discontinuous Galerkin finite element method for the time integration of a Cauchy problem second order ordinary differential equations. These equations typically arise after space semi-discretization of second order hyperbolic-type differential problems, e.g., wave, elastodynamics and acoustics equation. After introducing the new method, we analyze its well-posedness and prove a-priori error estimates in a suitable (mesh-dependent) norm. Numerical results are also presented to verify the theoretical estimates. space-time finite elements, discontinuous Galerkin methods, second order hyperbolic equations

1 Introduction

In this paper we develop a high-order discontinuous Galerkin scheme for the numerical approximation of ordinary differential equations that arise after space semi-discretization of second order hyperbolic problems. The applications we have in mind include, for example, acoustic, elastic and electromagnetic wave propagation phenomena. Traditional approaches for the numerical integration of (second order) ordinary differential systems rely on implicit and explicit finite difference, Runge-Kutta and Newmark schemes, see e.g., [31, 12, 35] for a

comprehensive review.
In many engineering applications explicit methods are in general preferred to implicit ones. In fact, although the latter are unconditionally stable, the former are less expensive from a computational point of view. The main drawback of explicit methods is the time-step limitation imposed by the Courant-Friedrichs-Lewy (CFL) condition. Such a constraint, which depends in general on the space discretization parameters and the media properties, can severely affect the computational efficiency.
A possible way to alleviate this limitation is to introduce suitable local time stepping (LTS) algorithms [21, 19, 14], using a small time-step only when needed. Another possibility is to adopt an explicit LTS method by extending the so-called arbitrary high-order derivatives discontinuous Galerkin (ADER-DG) approach [20, 43]. In this context, a proper time step can be tailored for each element of the time mesh. However, to correctly propagate the wave field from one element to the other an additional (computational demanding) synchronization process has to be taken into account.
In contrast with the above mentioned approaches, here we derive an implicit arbitrarily high order accurate time integration scheme based on a Discontinuous Galerkin (DG) spectral element (SE) approach.
DG methods [37, 32] have been firstly proposed to approximate (in space) hyperbolic problems [37] and then generalized to elliptic and parabolic equations [48, 6], see also [7, 25, 13, 38, 24, 18]. Relevant applications and analysis of DG schemes for the scalar wave equation can be found in [39, 22, 9] while for elastodynamics problems we refer the reader to [20, 49, 5, 33, 4, 3, 16]. The DG approach has also been used to solve initial-value problems. In time dependent problems, the information follows the positive direction of time and solutions are *casual* (they depend on the past but not on the future). In contrast with finite difference time integration schemes, for which the solution at the current step depends upon the previous steps, time discontinuous Galerkin methods applied over time slabs $[t_n, t_{n+1}]$ lead to a casual system in which the solution at the current time slab depends only upon the solution at t_n^-. By coupling discontinuous Galerkin discretizations in both space and time leads to a fully space-time finite element formulation. Relevant works on this topic concern both parabolic and hyperbolic problems, see e.g. [17, 45, 47].
For the latter, space-time finite elements are typically built upon reformulating the original problem as a system of first order equations (see, e.g., [26, 10, 29]). The latter can be seen as the result of space semi-discretization of first order hyperbolic problems or even second order hyperbolic problems in which the problem is formulated in term of the displacement (resp. velocity) and the stress (resp. strain) tensor fields.
To the best of our knowledge, only few recent results about finite element approximations of second order differential systems are available in literature, [28, 44, 2, 50, 46]. In [2] a new DG approach based on the solution of the scalar wave equation (and higher order differential equations) has been proposed and analyzed. The stabilization terms appearing in [2] introduced to penalize the jumps of the solution and its derivative across different time slabs are similar to those proposed in [26, 28, 44] where a Galerkin least square (GLS) approach is applied to stabilize the numerical scheme and prove its convergence. As an extension of the space-time formulation of [27], in [50] the authors present an enriched version of the space-time finite element method in order to incorporate in the same model multiple temporal scale features. A combination of continuous and discontinuous Galerkin time stepping approach is used in [46] to develop arbitrary order approximation for second order hyperbolic problems. Stability, convergence and accuracy is proved for scalar wave propagation with non-homogeneous

boundary conditions.

In the present work, a new DG method for the solution of systems of second order ordinary differential equations is presented. The resulting weak formulation is obtained by imposing the continuity of tractions and velocities across time-slabs weakly, without adding any extra GLS stabilization term. We show that the proposed formulation, in which the displacement field is the only unknown, is well posed and we prove *a-priori* stability and error estimates in a suitable mesh-dependent norm. The obtained time discontinuous scheme results in an implicit and unconditionally stable method. Moreover, allowing independent displacement interpolations between different time slabs, this method is naturally suited for an adaptive choice of the time discretization parameters, i.e., use of high order polynomials/small time steps only when the solution features sharp (temporal) gradients.

The paper is organized as follows. In Section 2 we formulate the problem, discretize it and analyze its well-posedness. Finally, we derive the corresponding algebraic system of equations. In Section 3 we carry out the convergence analysis providing suitable stability and error estimates. The application of the proposed method to the elastodynamics equations is described in Section 4. Here, the space-time finite element formulation is obtained combining the DGSE spatial discretization proposed in [5] to the one presented here for the time integration. Numerical results are shown in Section 5.

Throughout the paper we denote by $\|\mathbf{a}\|$ the Euclidean norm of a vector $\mathbf{a} \in \mathbb{R}^d$, $d \geq 1$ and by $\|A\|_\infty = \max_{i=1,\dots,m} \sum_{j=1}^{n} |a_{ij}|$, the ℓ^∞-norm of a matrix $A \in \mathbb{R}^{m\times n}$, $m, n \geq 1$. Moreover C denotes a generic positive constant that may take different values in different places, but is always independent of the discretization parameters. The notation $x \lesssim y$ means $x \leq Cy$ for a constant C as before. For a given $I \subset \mathbb{R}$, for any $v : I \to \mathbb{R}$ we denote by $L^p(I)$ and $H^p(I)$, $p \in \mathbb{N} \setminus 0$ the usual Lebesgue and Hilbert spaces, respectively and endow them with the usual norms, see [1]. For $p = 0$ we write $L^2(I)$ in place of $H^0(I)$. Finally, we use boldface type for vectorial functions. More precisely, the Lebesgue and Hilbert spaces of vector–valued functions are denoted by $\mathbf{L}^p(I) = [L^p(I)]^d$ and $\mathbf{H}^p(I) = [H^p(I)]^d$, respectively, $d \geq 1$.

2 A model problem and its discontinuous Galerkin spectral element approximation

In this section, we introduce a high-order discontinuous Galerkin spectral element method for second order ordinary differential equations, prove its well posedness and provide its algebraic form.

2.1 Problem statement and its DG discretization

For $T > 0$ we consider the following model problem: find $\mathbf{u} : (0, T] \to \mathbb{R}^d, d \geq 1$, such that

$$\ddot{\mathbf{u}}(t) + L\dot{\mathbf{u}}(t) + K\mathbf{u}(t) = \mathbf{f}(t) \qquad \forall t \in (0, T], \tag{1}$$

where $L, K \in \mathbb{R}^{d\times d}$ are symmetric, positive definite matrices and $\mathbf{f} \in \mathbf{L}^2(0,T]$. We supplement problem (1) with the following initial conditions:

$$\mathbf{u}(0) = \mathbf{u}_0, \qquad \dot{\mathbf{u}}(0) = \mathbf{u}_1, \tag{2}$$

where $\mathbf{u}_0, \mathbf{u}_1 \in \mathbb{R}^d$. Problem (1) is well posed and admits a unique solution $\mathbf{u} \in \mathbf{H}^2(0,T]$ in the interval $(0,T]$, see [30].

We partition the interval $I = (0,T]$ into N time slabs $I_n = (t_{n-1}, t_n]$ having length $\Delta t_n = t_n - t_{n-1}$, for $n = 1,..,N$, with $t_0 = 0$ and $t_N = T$, as it is shown in Figure 1.

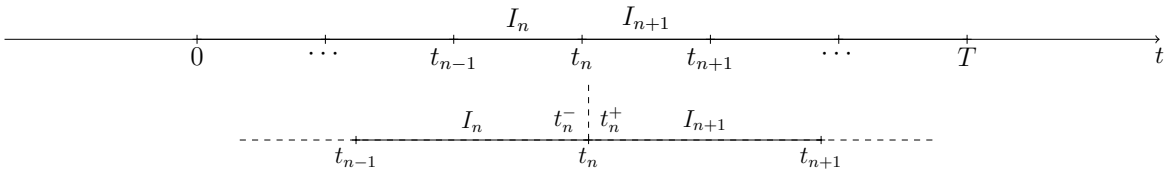

Figure 1: Example of time domain partition (top). Zoom of the time domain partition: values t_n^+ and t_n^- are also reported (bottom).

In the following we will use the notation:

$$(\mathbf{u}, \mathbf{v})_I = \int_I \mathbf{u}(s) \cdot \mathbf{v}(s)\, ds, \qquad \langle \mathbf{u}, \mathbf{v} \rangle_t = \mathbf{u}(t) \cdot \mathbf{v}(t),$$

where $\mathbf{a} \cdot \mathbf{b}$ indicates the euclidean scalar product between two vectors $\mathbf{a}, \mathbf{b} \in \mathbb{R}^d$. To deal with discontinuous functions, we also define, for (a regular enough) $\mathbf{v}$, the jump operator at t_n as

$$[\mathbf{v}]_n = \mathbf{v}(t_n^+) - \mathbf{v}(t_n^-), \quad \text{for } n \geq 0,$$

where

$$\mathbf{v}(t_n^\pm) = \lim_{\epsilon \to 0^\pm} \mathbf{v}(t_n + \epsilon), \quad \text{for } n \geq 0.$$

Implicit with the above definition is that

$$[\mathbf{v}]_0 = \mathbf{v}(0^+) - \mathbf{u}_0, \qquad [\dot{\mathbf{v}}]_0 = \dot{\mathbf{v}}(0^+) - \mathbf{u}_1.$$

Moreover, we use the symbols $\mathbf{v}_n^+ = \mathbf{v}(t_n^+)$ and $\mathbf{v}_n^- = \mathbf{v}(t_n^-)$ to represent the trace of (a regular enough) $\mathbf{v}$, taken within the interior of I_{n+1} and I_n, respectively (cf. Figure 1).
Next, following a time integration approach we incrementally build (on n) an approximation of the exact solution $\mathbf{u}$ on each time slab I_n. For this reason, we focus on the generic interval I_n, and assume the solution on I_{n-1} to be known. Note that $\mathbf{u} \in \mathbf{H}^2(I_n)$. If we multiply equation (1) by $\dot{\mathbf{v}}(t)$, being $\mathbf{v}(t)$ a regular enough function, we obtain

$$(\ddot{\mathbf{u}}, \dot{\mathbf{v}})_{I_n} + (L\dot{\mathbf{u}}, \dot{\mathbf{v}})_{I_n} + (K\mathbf{u}, \dot{\mathbf{v}})_{I_n} = (\mathbf{f}, \dot{\mathbf{v}})_{I_n}. \tag{3}$$

Next, since $\mathbf{u} \in \mathbf{H}^2(0,T)$, we observe that $[\mathbf{u}]_n = [\dot{\mathbf{u}}]_n = \mathbf{0}$, for $n = 1, \ldots, N$, we rewrite (3) adding suitable (strongly consistent) terms

$$(\ddot{\mathbf{u}}, \dot{\mathbf{v}})_{I_n} + (L\dot{\mathbf{u}}, \dot{\mathbf{v}})_{I_n} + (K\mathbf{u}, \dot{\mathbf{v}})_{I_n} + [\dot{\mathbf{u}}]_{n-1} \cdot \dot{\mathbf{v}}_{n-1}^+ + K[\mathbf{u}]_{n-1} \cdot \mathbf{v}_{n-1}^+ = (\mathbf{f}, \dot{\mathbf{v}})_{I_n}. \tag{4}$$

Taking to the right hand side the datum $\mathbf{f}$ and summing over all time slab we are able to define respectively the bilinear form $\mathcal{A} : \mathbf{H}^2(0,T) \times \mathbf{H}^2(0,T) \to \mathbb{R}$

$$\mathcal{A}(\mathbf{u},\mathbf{v}) = \sum_{n=1}^{N} \Big((\ddot{\mathbf{u}}, \dot{\mathbf{v}})_{I_n} + (L\dot{\mathbf{u}}, \dot{\mathbf{v}})_{I_n} + (K\mathbf{u}, \dot{\mathbf{v}})_{I_n} \Big) + \sum_{n=1}^{N-1} \Big([\dot{\mathbf{u}}]_n \cdot \dot{\mathbf{v}}_n^+ + K[\mathbf{u}]_n \cdot \mathbf{v}_n^+ \Big) + \dot{\mathbf{u}}_0^+ \cdot \dot{\mathbf{v}}_0^+ + K\mathbf{u}_0^+ \cdot \mathbf{v}_0^+, \quad (5)$$

and the linear functional $F : \mathbf{H}^2(0,T) \to \mathbb{R}$ as

$$F(\mathbf{v}) = \sum_{n=1}^{N} (\mathbf{f}, \dot{\mathbf{v}})_{I_n} + \mathbf{u}_1 \cdot \dot{\mathbf{v}}_0^+ + K\mathbf{u}_0 \cdot \mathbf{v}_0^+. \quad (6)$$

Notice that for $n = 1$, we implicitly adopted the convention that $\mathbf{u}_0^- = \mathbf{u}_0$ and $\dot{\mathbf{u}}_0^- = \mathbf{u}_1$. Next, we introduce the local finite dimensional space

$$\mathbf{V}_n^r = \{\mathbf{v} : I_n \to \mathbb{R}^d : \mathbf{v} \in [\mathbb{P}^r(I_n)]^d\},$$

where $\mathbb{P}^r(I_n)$ is the space of polynomials of degree greater than or equal to $r \geq 2$ on I_n. Then, introducing $\mathbf{r} = (r_1, ..., r_N) \in \mathbb{N}^N$ the polynomial degree vector, we can define the DG finite element space as

$$\mathcal{V}^{\mathbf{r}} = \{\mathbf{v} \in \mathbf{L}^2(0,T) : \mathbf{v}|_{I_n} \in \mathbf{V}_n^{r_n} \quad \forall\, n = 1, \ldots, N\},$$

whose dimension is $\sum_{n=1}^{N}(r_n + 1)d$. The DG formulation of problem (1)-(2) reads as follows: find $\mathbf{u}_{DG} \in \mathcal{V}^{\mathbf{r}}$ such that

$$\mathcal{A}(\mathbf{u}_{DG}, \mathbf{v}) = F(\mathbf{v}) \qquad \forall\, \mathbf{v} \in \mathcal{V}^{\mathbf{r}}. \quad (7)$$

The existence and uniqueness of the discrete solution $\mathbf{u}_{DG} \in \mathcal{V}^{\mathbf{r}}$ of problem (7) is a direct consequence of the following result.

Proposition 2.1. *The function* $|||\cdot||| : \mathcal{V}^{\mathbf{r}} \to \mathbb{R}^+$*, defined as*

$$|||\mathbf{v}|||^2 = \sum_{n=1}^{N} \|L^{\frac{1}{2}}\dot{\mathbf{v}}\|^2_{\mathbf{L}^2(I_n)} + \frac{1}{2}(\dot{\mathbf{v}}_0^+)^2 + \frac{1}{2}\sum_{n=1}^{N-1}\Big([\dot{\mathbf{v}}]_n\Big)^2 + \frac{1}{2}(\dot{\mathbf{v}}_T^-)^2 + \frac{1}{2}(K^{\frac{1}{2}}\mathbf{v}_0^+)^2 + \frac{1}{2}\sum_{n=1}^{N-1}\Big(K^{\frac{1}{2}}[\mathbf{v}]_n\Big)^2 + \frac{1}{2}(K^{\frac{1}{2}}\mathbf{v}_T^-)^2, \quad (8)$$

is a norm on $\mathcal{V}^{\mathbf{r}}$*.*

Proof. Since the absolute homogeneity and the subadditivity properties are satisfied, we just need to show that

$$|||\mathbf{v}||| = 0 \Leftrightarrow \mathbf{v} = \mathbf{0}.$$

The sufficient condition is trivial. We then show that $|||\mathbf{v}||| = 0$ implies $\mathbf{v} = \mathbf{0}$. Clearly, if $|||\mathbf{v}||| = 0$ then all the terms on the right hand side of (8) are null. In particular, from the

facts K and L are positive definite and $\|L^{\frac{1}{2}}\dot{\mathbf{v}}\|_{\mathbf{L}^2(I_0)} = 0$ and $(K^{\frac{1}{2}}\mathbf{v}_0^+)^2 = 0$ we conclude that $\mathbf{v}$ is such that

$$\begin{cases} \dot{\mathbf{v}}(t) = \mathbf{0} & \forall\, t \in I_0, \\ \mathbf{v}_0^+ = \mathbf{0}. \end{cases}$$

Therefore, we have that $\mathbf{v}(t)|_{I_0} = \mathbf{0}$. We now reason by induction, and consider the interval I_n, supposing $\mathbf{v}(t)|_{I_{n-1}} = \mathbf{0}$. From $|||\mathbf{v}||| = 0$ we have $(K^{\frac{1}{2}}[\mathbf{v}]_n)^2 = 0$, which yields $\mathbf{v}_n^+ = 0$. Indeed, we infer that $\mathbf{v}$ is such that

$$\begin{cases} \dot{\mathbf{v}}(t) = \mathbf{0} & \forall\, t \in I_n, \\ \mathbf{v}_n^+ = \mathbf{0}. \end{cases}$$

As result, we conclude that $\mathbf{v}$ is the null function on any interval I_n, $n = 0, \dots, N-1$, and the proof is complete. □

As a trivial consequence of Proposition 2.1 we have the following result.

Remark 1. *Taking* $\mathbf{u} = \mathbf{v}$ *in* (5) *and integrating by parts we obtain*

$$\mathcal{A}(\mathbf{v}, \mathbf{v}) = |||\mathbf{v}|||^2 \quad \forall\, \mathbf{v} \in \mathcal{V}^{\mathbf{r}},$$

i.e, the bilinear form $\mathcal{A}(\cdot,\cdot)$ *defined in* (5) *is coercive with respect to the norm* $|||\cdot|||$*, with coercivity constant* $\alpha = 1$*.*

Therefore, the following result holds.

Proposition 2.2. *Problem* (7) *admits a unique solution* $\boldsymbol{u}_{DG} \in \mathcal{V}^{\mathbf{r}}$*.*

The proof follows directly from Proposition 2.1 and the linearity of $\mathcal{A}(\cdot,\cdot)$.

2.2 Algebraic formulation

We derive here the algebraic formulation corresponding to problem (4) for the time slab I_n, where a local degree r_n is employed.
We remark indeed that the employment of discontinuous functions between a node t_n allows to compute the solution of the problem separately for one time slab at a time. For this reason in this section we focus on the generic interval I_n, and to this aim we introduce a basis $\{\psi^\ell(t)\}_{\ell=1,\dots,r_n+1}$ for the polynomial space $\mathbb{P}^r_n(I_n)$ and define $D = d(r_n + 1)$ the dimension of the local finite dimensional space $\mathbf{V}_n^{r_n}$. We also introduce the vectorial basis $\{\mathbf{\Psi}_i^\ell(t)\}_{i=1,\dots,d}^{\ell=1,\dots,r_n+1}$, where

$$\{\mathbf{\Psi}_i^\ell(t)\}_j = \begin{cases} \psi^\ell(t) & \ell = 1, \dots, r_n+1, \quad \text{if } i = j, \\ 0 & \ell = 1, \dots, r_n+1, \quad \text{if } i \neq j. \end{cases}$$

Using the notation just introduced we can write the trial function $\mathbf{u}_n = \mathbf{u}_{DG|_{I_n}} \in \mathbf{V}_n^{r_n}$ as a linear combination of the basis functions, i.e.,

$$\mathbf{u}_n(t) = \sum_{j=1}^{d} \sum_{m=1}^{r_n+1} \alpha_j^m \mathbf{\Psi}_j^m(t),$$

where $\alpha_j^m \in \mathbb{R}$ for $j = 1, \dots, d$ and $m = 1, \dots, r_n + 1$.
Next, we write equation (7) for any test function $\mathbf{\Psi}_i^\ell(t), i = 1, \dots, d, \ell = 1, \dots, r_n+1$, obtaining the algebraic system

$$A\mathbf{U}_n = \mathbf{F}_n,$$

where $\mathbf{U}_n, \mathbf{F}_n \in \mathbb{R}^D$ are the vectors corresponding to the solution and the on the interval I_n and $A \in \mathbb{R}^{D\times D}$ is the related local stiffness matrix.
We next detail the structure of the matrix A. To this aim we define the following local matrices for $\ell, m = 1, \dots, r_n + 1$,

$$M^1_{\ell m} = (\ddot{\psi}^m, \dot{\psi}^\ell)_{I_n}, \qquad M^2_{\ell m} = (\dot{\psi}^m, \dot{\psi}^\ell)_{I_n}, \qquad M^3_{\ell m} = (\psi^m, \dot{\psi}^\ell)_{I_n},$$
$$M^4_{\ell m} = \langle \dot{\psi}^m, \dot{\psi}^\ell \rangle_{t^+_{n-1}}, \quad M^5_{\ell m} = \langle \psi^m, \psi^\ell \rangle_{t^+_{n-1}}.$$

Therefore, setting

$$M = M^1 + M^4,$$
$$B_{ij} = L_{ij}M^2 + K_{ij}\left(M^3 + M^5\right), \qquad i, j = 1, ..., d,$$

with $M, B_{ij} \in \mathbb{R}^{(r_n+1)\times(r_n+1)}$ for any $i, j = 1, \dots, d$, we can rewrite the matrix A as

$$A = \begin{vmatrix} M & 0 & \cdots & 0 \\ 0 & M & & \vdots \\ \vdots & & \ddots & 0 \\ 0 & \cdots & 0 & M \end{vmatrix} + \begin{vmatrix} B_{11} & B_{12} & \cdots & B_{1d} \\ B_{21} & B_{22} & & \vdots \\ \vdots & & \ddots & \\ B_{d1} & \cdots & & B_{dd} \end{vmatrix}. \tag{9}$$

Its structure clearly depends on the sparsity pattern of the matrices L and K.

3 Convergence analysis

In this section we first analyze the stability of the DG spectral element method (7) and then we prove *a-priori* error estimates.

3.1 Stability analysis

Let $\mathbf{u}_{DG} \in \mathcal{V}^{\mathbf{r}}$ be the solution of (7). Then we have the following result

Proposition 3.1. *Let $\mathbf{f} \in \boldsymbol{L}^2(0,T]$ and $\mathbf{u}_0, \mathbf{u}_1 \in \mathbb{R}^d$. Then, it holds*

$$|||\mathbf{u}_{DG}||| \lesssim \left(\|L^{-\frac{1}{2}}\mathbf{f}\|^2_{\mathbf{L}^2(0,T)} + (K^{\frac{1}{2}}\mathbf{u}_0)^2 + (\mathbf{u}_1)^2\right)^{\frac{1}{2}}. \tag{10}$$

Proof. Using the definition of the norm $|||\cdot|||$ in (8) and arithmetic-geometric inequality we have

$$|||\mathbf{u}_{DG}|||^2 = \mathcal{A}(\mathbf{u}_{DG}, \mathbf{u}_{DG}) = \sum_{n=1}^{N} (\mathbf{f}, \dot{\mathbf{u}}_{DG})_{I_n} + \mathbf{u}_1 \cdot \dot{\mathbf{u}}_{DG}(0^+) + K\mathbf{u}_0 \cdot \mathbf{u}_{DG}(0^+)$$
$$\leq \frac{1}{2}\sum_{n=1}^{N}\left(\|L^{-\frac{1}{2}}\mathbf{f}\|^2_{\mathbf{L}^2(I_n)} + \|L^{\frac{1}{2}}\dot{\mathbf{u}}_{DG}\|^2_{\mathbf{L}^2(I_n)}\right)$$
$$+ \mathbf{u}_1^2 + \frac{1}{4}\dot{\mathbf{u}}^2_{DG}(0^+) + (K^{\frac{1}{2}}\mathbf{u}_0)^2 + \frac{1}{4}(K^{\frac{1}{2}}\mathbf{u}_{DG}(0^+))^2,$$

that is

$$\frac{1}{2}|||\mathbf{u}_{DG}|||^2 \leq \frac{1}{2}\sum_{n=1}^{N} \|L^{-\frac{1}{2}}\mathbf{f}\|^2_{\mathbf{L}^2(I_n)} + \mathbf{u}_1^2 + (K^{\frac{1}{2}}\mathbf{u}_0)^2,$$

and the proof is complete. □

3.2 Error estimates

In this section, we derive *a priori* error estimates in the $|||\cdot|||$ norm defined in (8). We start by introducing some preliminary definitions and results.

Definition 1. *Let $I = (-1,1)$. For a function $u \in H^2(I)$ we define $\Pi^r u \in \mathbb{P}^r(I)$, $r \geq 2$, by the $r+1$ conditions*

$$(\Pi^r u - u)(1) = 0, \tag{11a}$$
$$(\Pi^r u - u)(-1) = 0, \tag{11b}$$
$$(\Pi^r u - u)'(1) = 0, \tag{11c}$$
$$\int_I (u - \Pi^r u) q \, dt = 0, \quad \forall q \in \mathbb{P}^{r-3}(I). \tag{11d}$$

For $r = 2$, only the first three conditions (11a)–(11c) *are necessary.*

In the following, we denote by $\{L_i\}_{i\geq 0}$, $L_i \in \mathbb{P}^i(I)$, the Legendre polynomials on $I = (-1,1)$.

Lemma 3.1. *The operator $\Pi^r : H^2(I) \to \mathbb{P}^r(I)$ in Definition 1 is well defined.*

Proof. Assume that u_1 and u_2 are two polynomials in $\mathbb{P}^r(I)$ which satisfy (11a)–(11d). In particular, we have $u_1(\pm 1) = u_2(\pm 1)$ and $u_1'(1) = u_2'(1)$. The difference $u_1 - u_2$ can be expanded as $u_1 - u_2 = \sum_{i=0}^{r} c_i L_i$ with $c_i = \int_I (u_1 - u_2) L_i \, dt \in \mathbb{R}$. From (11d) it easily follows that $c_k = 0$ for $k = 0, \ldots, r-3$, using the orthogonality properties of the Legendre polynomials in I. The difference $u_1 - u_2$ is therefore given by $u_1 - u_2 = c_{r-2}L_{r-2} + c_{r-1}L_{r-1} + c_r L_r$, $c_r \in \mathbb{R}$. Because of conditions (11a)–(11c), we have $c_{r-2} = c_{r-1} = c_r = 0$, which proves the uniqueness of a polynomial satisfying the conditions in Definition 1. The existence follows by construction setting

$$\Pi^r u = \sum_{i=0}^{r-3} u_i L_i + (u_{r-2} + u^*_{r-2})L_{r-2} + (u_{r-1} + u^*_{r-1})L_{r-1} + (u_r + u^*_r)L_r, \tag{12}$$

where

$$u^*_{r-2} = \frac{r^2}{2(2r-1)} \sum_{j=r+1}^{\infty} u_j + \frac{r}{2(2r-1)} \sum_{j=r+1}^{\infty} (-1)^{r+j} u_j - \frac{1}{(2r-1)} \sum_{j=r+1}^{\infty} \frac{j(j+1)}{2} u_j \tag{13}$$

$$u^*_{r-1} = \frac{1}{2} \sum_{j=r+1}^{\infty} u_j + \frac{1}{2} \sum_{j=r+1}^{\infty} (-1)^{r+j} u_j \tag{14}$$

$$u^*_{r} = -\frac{(r-1)^2}{2(2r-1)} \sum_{j=r+1}^{\infty} u_j + \frac{(r-1)}{2(2r-1)} \sum_{j=r+1}^{\infty} (-1)^{r+j} u_j + \frac{1}{(2r-1)} \sum_{j=r+1}^{\infty} \frac{j(j+1)}{2} u_j \tag{15}$$

where $u = \sum_{i=0}^{\infty} u_i L_i$ is the Legendre expansion of u. The derivation of coefficients (13)–(15) is detailed in Appendix. □

On an arbitrary interval $I = (a, b)$ with $\Delta t = b - a > 0$ we define Π_I^r via the linear map $Q : (-1, 1) \to (a, b)$, $\xi \to y = \frac{1}{2}(a + b + \xi \Delta t)$ as $\Pi_I^r u = [\Pi^r (u \circ Q)] \circ Q^{-1}$.
Now, we analyze the properties of the projector Π^r.

Lemma 3.2. *For $r \geq 2$ and $u \in H^2(I)$ we have*

$$\|\Pi^r u\|_{L^2(I)} \lesssim \|u\|_{H^2(I)}.$$

Proof. We develop u' into the Legendre series $u' = \sum_{i=0}^{\infty} b_i L_i$ with coefficients $b_i \in \mathbb{R}$. Then u can be written as $u(t) = \sum_{i=0}^{\infty} b_i \int_{-1}^{t} L_i(s)\, ds + u(-1)$. Recalling that $L_0(t) = 1$, $L_1(t) = t$, and $\int_{-1}^{t} L_i(s)\, ds = \frac{1}{2i+1}(L_{i+1}(t) - L_{i-1}(t))$ for $i \geq 1$ we can write

$$u = (b_0 - \frac{b_1}{3} + u(-1))L_0 + \sum_{i=1}^{\infty} \left(\frac{b_{i-1}}{2i-1} - \frac{b_{i+1}}{2i+3} \right) L_i$$

where

$$\begin{aligned} u_0 &= b_0 - \frac{b_1}{3} + u(-1) \\ u_i &= \frac{b_{i-1}}{2i-1} - \frac{b_{i+1}}{2i+3}, \quad \text{for } i \geq 1. \end{aligned}$$

See also [40]. Consequently, we have for $r \geq 1$,

$$\begin{aligned} \sum_{i=r+1}^{\infty} u_i &= \sum_{i=r+1}^{\infty} \left(\frac{b_{i-1}}{2i-1} - \frac{b_{i+1}}{2i+3} \right) = \sum_{i=r}^{\infty} \frac{b_i}{2i+1} - \sum_{i=r+2}^{\infty} \frac{b_i}{2i+1} \\ &= \frac{b_r}{2r+1} + \frac{b_{r+1}}{2r+3}. \end{aligned}$$

This leads to

$$\left| \sum_{i=r+1}^{\infty} u_i \right|^2 \lesssim \frac{|b_r|^2}{(2r+1)^2} + \frac{|b_{r+1}|^2}{(2r+3)^2} \lesssim r^{-1} \|u'\|_{L^2(I)}^2. \tag{16}$$

Next, we repeat the previous argument for u'' expressing it in term of the Legendre expansion $u'' = \sum_{i=0}^{\infty} c_i L_i$ with coefficients $c_i \in \mathbb{R}$. Then, u' can be written as $u'(t) = \sum_{i=0}^{\infty} c_i \int_{-1}^{t} L_i(s)\, ds + u'(-1)$, where the expansion coefficients c_i are related to coefficients b_i through the relations

$$\begin{aligned} b_0 &= c_0 - \frac{c_1}{3} + u'(-1) \\ b_i &= \frac{c_{i-1}}{2i-1} - \frac{c_{i+1}}{2i+3}, \quad \text{for } i \geq 1. \end{aligned}$$

Using the above expression we can write the coefficients u_i in term of c_i as

$$\begin{aligned} u_0 &= \frac{2}{3}c_0 - \frac{1}{3}c_1 + \frac{1}{5}c_2 + u(-1) + u'(-1) \\ u_1 &= c_0 - \frac{6}{15}c_1 + \frac{1}{35}c_3 + u'(-1) \\ u_i &= \frac{c_{i-2}}{(2i-1)(2i-3)} - \frac{2c_i}{(2i-1)(2i+3)} + \frac{c_{i+2}}{(2i+3)(2i+5)}, \quad \text{for } i \geq 2. \end{aligned}$$

Consequently, we have for $r \geq 1$

$$\sum_{i=r+1}^{\infty} i(i+1)u_i = \frac{(r+1)(r+2)}{(2r-1)(2r+1)}c_{r-1} + \frac{(r+2)(r+3)}{(2r+1)(2r+3)}c_r \tag{17}$$

$$- \frac{r(r-1)}{(2r+1)(2r+3)}c_{r+1} - \frac{r(r+1)}{(2r+3)(2r+5)}c_{r+2}. \tag{18}$$

See the Appendix for the detailed calculation. This yields

$$\left|\sum_{i=r+1}^{\infty} i(i+1)u_i\right|^2 \lesssim r\left(\frac{|c_{r-2}|^2}{(2r-1)} + \frac{|c_r|^2}{(2r+1)} + \frac{|c_{r+1}|^2}{(2r+3)} + \frac{|c_{r+2}|^2}{(2r+5)}\right) \lesssim r\|u''\|^2_{L^2(I)}. \tag{19}$$

Now, using (16) and (19) we can estimate the expansion coefficients of the projection $\Pi^r u$ in (13)–(15). In particular, we have that

$$\begin{aligned}
|u^*_{r-2}|^2 &\lesssim \frac{r^4}{(2r-1)^2}\left|\sum_{j=r+1}^{\infty} u_j\right|^2 + \frac{r^2}{(2r-1)^2}\left|\sum_{j=r+1}^{\infty}(-1)^{r+j}u_j\right|^2 + \frac{1}{(2r-1)^2}\left|\sum_{j=r+1}^{\infty} j(j+1)u_j\right|^2 \\
&\lesssim r\|u'\|^2_{L^2(I)} + r^{-1}\|u'\|^2_{L^2(I)} + r^{-1}\|u''\|^2_{L^2(I)} \\
&\lesssim r\|u'\|^2_{L^2(I)} + r^{-1}\|u''\|^2_{L^2(I)}.
\end{aligned}$$

A similar result holds for u^*_r while for u^*_{r-1} it is easy to see that

$$|u^*_{r-1}|^2 \lesssim \left|\sum_{j=r+1}^{\infty} u_j\right|^2 + \left|\sum_{j=r+1}^{\infty}(-1)^{r+j}u_j\right|^2 \lesssim r^{-1}\|u'\|^2_{L^2(I)}.$$

The proof follows by using the definition of the projector operator Π^r and by triangle inequality. Indeed, we have

$$\begin{aligned}
\|\Pi^r u\|^2_{L^2(I)} &\lesssim \|\sum_{i=0}^{r} u_i L_i\|^2_{L^2(I)} + |u^*_{r-2}|^2\|L_{r-2}\|^2_{L^2(I)} + |u^*_{r-1}|^2\|L_{r-1}\|^2_{L^2(I)} + |u^*_r|^2\|L_r\|^2_{L^2(I)} \\
&\lesssim \|u\|^2_{L^2(I)} + \|u'\|^2_{L^2(I)} + r^{-2}\|u''\|^2_{L^2(I)} \lesssim \|u\|^2_{H^2(I)}
\end{aligned}$$

□

The following property holds for the projector Π^r in Definition 1.

Lemma 3.3. *Let $u \in H^2(I)$ and let $u = \sum_{i=0}^{\infty} u_i L_i$ be the Legendre expansion of u with coefficients $u_i \in \mathbb{R}$. For $r \geq 2$ we denote by P^r the $L^2(I)$-projection onto $\mathbb{P}^r(I)$. There holds*

$$\begin{aligned}
\|u - \Pi^r u\|^2_{L^2(I)} \lesssim \|u - P^r u\|^2_{L^2(I)} &+ r|u(1) - P^r u(1)|^2 \\
&+ r^{-1}|u(-1) - P^r u(-1)|^2 + r^{-3}|u'(1) - (P^r u)'(1)|^2.
\end{aligned} \tag{20}$$

Proof. We start by expressing $u - \Pi^r u = (u - P^r u) + (P^r u - \Pi^r u)$. Using now definitions (12) and the orthogonality properties of the Legendre polynomials we have that

$$\|P^r u - \Pi^r u\|^2_{L^2(I)} = |u^*_{r-2}|^2 \|L_{r-2}\|^2_{L^2(I)} + |u^*_{r-1}|^2 \|\|L_{r-1}\|^2_{L^2(I)} + |u^*_r|^2 \|L_r\|^2_{L^2(I)},$$

and then

$$\|P^r u - \Pi^r u\|^2_{L^2(I)} \lesssim r^{-1}(|u^*_{r-2}|^2 + |u^*_{r-1}|^2 + |u^*_r|^2). \tag{21}$$

Next, using definitions (13)–(15), triangle and arithmetic-geometric inequality and definition of P^r, we can estimate the terms on the right and side in (21) as

$$\begin{aligned}
|u^*_{r-2}|^2 &\lesssim r^2 \left|u(1) - P^r u(1)\right|^2 + \left|u(-1) - P^r u(-1)\right|^2 + r^{-2}\left|u'(1) - (P^r u)'(1)\right|^2, \\
|u^*_{r-1}|^2 &\lesssim \left|u(1) - P^r u(1)\right|^2 + \left|u(-1) - P^r u(-1)\right|^2, \\
|u^*_r|^2 &\lesssim r^2 \left|u(1) - P^r u(1)\right|^2 + \left|u(-1) - P^r u(-1)\right|^2 + r^{-2}\left|u'(1) - (P^r u)'(1)\right|^2.
\end{aligned}$$

The thesis follows by using the above inequalities into (21) and by application of the triangle inequality. □

We recall the following approximation result from [8], see also [41].

Proposition 3.2. *For every arbitrary interval $I = (a, b)$ with $\Delta t = b - a > 0$ and $u \in H^s(I)$ there exist a constant C, independent of $u, r, \Delta t$ and a sequence $\{P^r u\}_{r\geq 1}$, with each $P^r u \in \mathbb{P}^r(I)$ such that, for any $0 \leq q \leq s$,*

$$\|u - P^r u\|_{H^q(I)} \lesssim \frac{\Delta t^{\mu - q}}{r^{s-q}} \|u\|_{H^s(I)} \quad s \geq 0, \tag{22}$$

$$\|u - P^r u\|_{L^2(\partial I)} \lesssim \frac{\Delta t^{\mu - \frac{1}{2}}}{r^{s-\frac{1}{2}}} \|u\|_{H^s(I)} \quad s > \frac{1}{2}, \tag{23}$$

$$\|u - P^r u\|_{H^1(\partial I)} \lesssim \frac{\Delta t^{\mu - \frac{3}{2}}}{r^{s-\frac{3}{2}}} \|u\|_{H^s(I)} \quad s > \frac{3}{2}, \tag{24}$$

where $\mu = \min(r + 1, s)$.

.

The application of Proposition 3.2 in Lemma 3.3 and scaling arguments gives estimates for Π^r_I.

Lemma 3.4. *Let $I = (a, b)$ with $\Delta t = b - a$ and let $u \in H^s(I)$, with $s \geq 2$. There holds*

$$\|u - \Pi^r_I u\|_{L^2(I)} \lesssim \frac{\Delta t^{\mu - \frac{3}{2}}}{r^{s-1}} \|u\|_{H^s(I)}, \tag{25}$$

where $\mu = \min(r + 1, s)$.

Proof. By application of Lemma 3.3 to Π^r_I we have

$$\begin{aligned}
\|u - \Pi^r_I u\|^2_{L^2(I)} &\leq \|u - P^r_I u\|^2_{L^2(I)} + \|P^r_I u - \Pi^r_I u\|^2_{L^2(I)} \\
&\lesssim \|u - P^r_I u\|^2_{L^2(I)} + r|u(b) - P^r_I u(b)|^2 \\
&\qquad + r^{-1}|u(a) - P^r_I u(a)|^2 + r^{-3}|u'(b) - (P^r_I u)'(b)|^2.
\end{aligned}$$

Applying estimates (22)–(24) to the above equation we obtain the proof, i.e.,

$$\|u - \Pi_I^r u\|_{L^2(I)}^2 \leq \frac{\Delta t^{2\mu}}{r^{2s}} \|u\|_{H^s(I)}^2 + \frac{\Delta t^{2\mu-3}}{r^{2s-2}} \|u\|_{H^s(I)}^2 \lesssim \frac{\Delta t^{2\mu-3}}{r^{2s-2}} \|u\|_{H^s(I)}^2.$$

□

As a direct consequence of the above Lemma we have the following result.

Corollary 1. *Under the same hypotheses of Lemma 3.4 it holds*

$$\|(u - \Pi_I^r u)'\|_{L^2(I)} \lesssim \frac{\Delta t^{\mu-\frac{3}{2}}}{r^{s-2}} \|u\|_{H^s(I)}, \tag{26}$$

$$\|(u - \Pi_I^r u)''\|_{L^2(I)} \lesssim \frac{\Delta t^{\mu-2}}{r^{s-3}} \|u\|_{H^s(I)}, \tag{27}$$

where $\mu = \min(r+1, s)$.

Proof. We prove inequality (26), but with similar arguments it is possible to obtain (27). We start by observing that $\phi = P_I^r u - \Pi_I^r u \in \mathbb{P}^r(I)$. Then, it holds (cfr. [11, Lemma 2.1])

$$\|\phi'\|_{L^2(I)} \lesssim r^2 \|\phi\|_{L^2(I)}.$$

The thesis follows by applying the above inequality and estimates (22)–(24) to the following

$$\|(u - \Pi_I^r u)'\|_{L^2(I)}^2 \leq \|(u - P_I^r u)'\|_{L^2(I)}^2 + \|(P_I^r u - \Pi_I^r u)'\|_{L^2(I)}^2.$$

□

Before proving the main result of this section we notice that if $\mathbf{v} \in \mathbf{H}^s(I)$, for $s \geq 2$, then its projection $\Pi_I^r \mathbf{v} \in [\mathbb{P}^r(I)]^d$ is defined according to (11a)–(11d) and the same kind of estimates given in (25), (26) and (27) hold.
Now, let $I = (0, T)$, $\mathbf{u} \in \mathbf{H}^s(0, T]$ for $s \geq 2$ be the solution of (3) and let $\Pi_I^{\mathbf{r}} \mathbf{u} \in \mathcal{V}^{\mathbf{r}}$ be its projection such that $\Pi_I^{\mathbf{r}} \mathbf{u}_{|_{I_n}} = \Pi_{I_n}^{r_n} \mathbf{u} \in \mathbf{V}_n^{r_n}$ is defined according (11a)–(11d), for $n = 1, ..., N$. Then, it is easy to see that for $n = 1, ..., N$ it holds

$$(\mathbf{u} - \Pi_I^{\mathbf{r}})(t_n) = 0, \tag{28}$$

$$(\mathbf{u} - \Pi_I^{\mathbf{r}})'(t_n) = 0, \tag{29}$$

$$(\mathbf{u} - \Pi_I^{\mathbf{r}}, q)_{I_n} = 0, \qquad \forall\, q \in \mathbb{P}^{r_n - 3}(I_n). \tag{30}$$

Finally, we observe that (7) is strongly consistent [34]. Indeed, it holds

$$\mathcal{A}(\mathbf{u} - \mathbf{u}_{DG}, \mathbf{v}) = 0 \qquad \forall\, \mathbf{v} \in \mathcal{V}^{\mathbf{r}}. \tag{31}$$

We are now ready to prove the following convergence result.

Theorem 1. *Let* $\mathbf{u}$ *be the solution of* (1)-(2) *and let* $\mathbf{u}_{DG} \in \mathcal{V}^{\mathbf{r}}$ *be its finite element approximation. If* $\mathbf{u}|_{I_n} \in \mathbf{H}^{s_n}(I_n)$, *for any* $n = 1, ..., N$ *with* $s_n \geq 2$, *then it holds*

$$|||\mathbf{u} - \mathbf{u}_{DG}||| \lesssim \sum_{n=1}^{N} \frac{\Delta t_n^{\mu-\frac{3}{2}}}{r_n^{s_n-3}} \|\mathbf{u}\|_{\mathbf{H}^{s_n}(I_n)} \tag{32}$$

where $\mu_n = \min(r_n + 1, s_n)$ *for any* $n = 1, ..., N$ *and the hidden constant depends on the norm of the matrices* L *and* K.

Proof. We define the error on the interval $I = (0,T)$ as $\mathbf{e} = \mathbf{u} - \mathbf{u}_{DG}$, and we split it as $\mathbf{e} = \mathbf{e}^\pi + \mathbf{e}^h$, where $\mathbf{e}^\pi$ is the projection error while $\mathbf{e}^h \in \mathcal{V}^{\mathbf{r}}$ is the remainder, i.e.,

$$\mathbf{e}^\pi = \mathbf{u} - \Pi_I^{\mathbf{r}}\mathbf{u} \qquad \text{and} \qquad \mathbf{e}^h = \Pi_I^{\mathbf{r}}\mathbf{u} - \mathbf{u}_{DG}.$$

Clearly, we have $|||\mathbf{e}||| \leq |||\mathbf{e}^\pi||| + |||\mathbf{e}^h|||$. By exploiting properties (28)–(30) and by employing estimates (26) and (27) we can bound the term $|||\mathbf{e}^\pi|||$ as

$$\begin{aligned}
|||\mathbf{e}^\pi|||^2 &= \sum_{n=1}^{N} \|L^{\frac{1}{2}}\dot{\mathbf{e}}^\pi\|^2_{L^2(I_n)} + \frac{1}{2}\sum_{n=1}^{N} \dot{\mathbf{e}}^\pi(t_{n-1}^+)^2 = \sum_{n=1}^{N} \|L^{\frac{1}{2}}\dot{\mathbf{e}}^\pi\|^2_{L^2(I_n)} + \frac{1}{2}\sum_{n=1}^{N}\left(-\int_{t_{n-1}}^{t_n} \ddot{\mathbf{e}}^\pi(s)\,ds\right)^2 \\
&\lesssim \sum_{n=1}^{N}\left(\|\dot{\mathbf{e}}^\pi\|^2_{L^2(I_n)} + \Delta t\|\ddot{\mathbf{e}}^\pi\|^2_{L^2(I_n)}\right) \\
&\lesssim \sum_{n=1}^{N} \frac{\Delta t_n^{2\mu_n-3}}{r^{2s_n-6}}\|\mathbf{u}\|^2_{H^{s_n}(I_n)},
\end{aligned} \tag{33}$$

where $\mu_n = \min(r_n+1, s_n)$ for any $n = 1, ..., N$. For the term $|||\mathbf{e}^h|||$ the Galerkin orthogonality (31) leads to

$$\begin{aligned}
|||\mathbf{e}^h|||^2 &= \mathcal{A}(\mathbf{e}^h, \mathbf{e}^h) = -\mathcal{A}(\mathbf{e}^\pi, \mathbf{e}^h) \\
&= -\sum_{n=1}^{N}\Big((\ddot{\mathbf{e}}^\pi, \dot{\mathbf{e}}^h)_{I_n} + (L\dot{\mathbf{e}}^\pi, \dot{\mathbf{e}}^h)_{I_n} + (K\mathbf{e}^\pi, \dot{\mathbf{e}}^h)_{I_n} + [\dot{\mathbf{e}}^\pi]_n \cdot \dot{\mathbf{e}}^h(t_n^+) + K[\mathbf{e}^\pi]_n \cdot \mathbf{e}^h(t_n^+)\Big) \\
&\qquad - \dot{\mathbf{e}}^\pi(t_0^+)\cdot\dot{\mathbf{e}}^h(t_0^+) - K\mathbf{e}^\pi(t_0^+)\cdot\mathbf{e}^h(t_0^+).
\end{aligned}$$

Integrating by parts the term $(\ddot{\mathbf{e}}^\pi, \dot{\mathbf{e}}^h)_{I_n}$ and rearranging the addends we obtain

$$\begin{aligned}
|||\mathbf{e}^h|||^2 &= \sum_{n=1}^{N}\Big((\dot{\mathbf{e}}^\pi, \ddot{\mathbf{e}}^h)_{I_n} - (L\dot{\mathbf{e}}^\pi, \dot{\mathbf{e}}^h)_{I_n} - (K\mathbf{e}^\pi, \dot{\mathbf{e}}^h)_{I_n}\Big) \\
&\quad + \sum_{n=1}^{N-1}\Big([\dot{\mathbf{e}}^h]_n \cdot \dot{\mathbf{e}}^\pi(t_n^-) - K[\mathbf{e}^\pi]_n \cdot \mathbf{e}^h(t_n^+)\Big) - \dot{\mathbf{e}}^\pi(T^-)\cdot\dot{\mathbf{e}}^h(T^-) - K\mathbf{e}^\pi(0^+)\cdot\mathbf{e}^h(0^+).
\end{aligned}$$

Using now properties (28)–(30) into the above equation yields

$$|||\mathbf{e}^h|||^2 = \sum_{n=1}^{N}\Big(-(L\dot{\mathbf{e}}^\pi, \dot{\mathbf{e}}^h)_{I_n} - (K\mathbf{e}^\pi, \dot{\mathbf{e}}^h)_{I_n}\Big).$$

Applying Cauchy-Schwarz and arithmetic-geometric inequalities and using estimates (25) and (26) it is easy to obtain

$$|||\mathbf{e}^h|||^2 \lesssim \sum_{n=1}^{N}\Big(\|\dot{\mathbf{e}}^\pi\|^2_{L^2(In)} + \|\mathbf{e}^\pi\|^2_{L^2(In)}\Big) \lesssim \sum_{n=1}^{N}\frac{\Delta t_n^{2\mu_n-3}}{r^{2s_n-4}}\|\mathbf{u}\|^2_{H^{s_n}(I_n)} \tag{34}$$

where the hidden constant depends on the norms $\|L^{\frac{1}{2}}\|_\infty$ and $\|L^{-\frac{1}{2}}K\|_\infty$ and $\mu_n = \min(r_n + 1, s_n)$ for any $n = 1, ..., N$. Putting together estimates (33) and (34) we have

$$|||\mathbf{u} - \mathbf{u}_{DG}||| \lesssim \sum_{n=1}^{N}\frac{\Delta t_n^{\mu_n-\frac{3}{2}}}{r^{s_n-3}}\|\mathbf{u}\|_{H^{s_n}(I_n)},$$

with $\mu_n = \min(r_n + 1, s_n)$ for any $n = 1, ..., N$. □

As a consequence of this result we obtain the following.

Corollary 2. *Under the same assumptions of Theorem 1, suppose moreover that* $\Delta t_n = \Delta t$, $r_n = r$ *and* $s_n = s$ *for* $n = 1, ..., N$. *Then, it holds*

$$|||\mathbf{u} - \mathbf{u}_{DG}||| \lesssim \frac{\Delta t^{r-\frac{1}{2}}}{r^{s-3}} \|\mathbf{u}\|_{\mathbf{H}^s(0,T)},$$

where the hidden constant depends on the norm of the matrices L *and* K.

4 Application to the elastodynamics problem

In this section, we apply the method presented in Section 2 to the simulation of elastic wave propagations in heterogeneous media. In particular, we will adopt the DG method previously developed to handle the time integration of the second order differential system arising after space discretization obtained with the DGSE method proposed in [5]. Since the focus of the paper is on time integration, here we simply report the mathematical model of linear visco-elasticity and the algebraic linear system resulting after the space discretization obtained employing the DGSE scheme of [5]. Finally, some numerical results are discussed.

4.1 Mathematical modelling of seismic wave propagations and its algebraic formulation

For a given open bounded domain $\Omega \subset \mathbb{R}^m$, $m = 2, 3$, we consider the following problem: for $T > 0$ find $\mathbf{u} : \Omega \times [0, T] \to \mathbb{R}^m$ such that

$$\rho \partial_{tt}\mathbf{u} + 2\rho\zeta\partial_t\mathbf{u} + \rho\zeta^2\mathbf{u} - \nabla \cdot \boldsymbol{\sigma} = \mathbf{f}, \qquad \text{in } \Omega \times (0, T], \tag{35a}$$

$$\mathbf{u} = \mathbf{0}, \qquad \text{on } \Gamma_D \times (0, T], \tag{35b}$$

$$\boldsymbol{\sigma}\mathbf{n} = \mathbf{0}, \qquad \text{on } \Gamma_N \times (0, T], \tag{35c}$$

$$\partial_t\mathbf{u} = \mathbf{u}_1, \qquad \text{in } \Omega \times \{0\}, \tag{35d}$$

$$\mathbf{u} = \mathbf{u}_0, \qquad \text{in } \Omega \times \{0\}, \tag{35e}$$

where $\overline{\partial\Omega} = \overline{\Gamma_D} \cup \overline{\Gamma_N}$ with $\Gamma_D \cap \Gamma_N = \emptyset$, $\mathbf{f} \in L^2((0, T]; \mathbf{L}^2(\Omega))$ is the source term, and $\rho \in L^\infty(\Omega)$ is such that $\rho = \rho(\mathbf{x}) > 0$ for almost any $\mathbf{x} \in \Omega$. The function $\zeta = \zeta(\mathbf{x}) > 0$ is a decay factor whose dimension is the inverse of time, and is a piecewise constant function, then $\zeta \in L^\infty(\Omega)$. We suppose the stress tensor $\boldsymbol{\sigma}$ to be related to the strain tensor $\boldsymbol{\varepsilon}(\mathbf{u}) = \frac{1}{2}\left(\nabla\mathbf{u} + \nabla\mathbf{u}^T\right)$ through the Hooke's law, that is

$$\boldsymbol{\sigma} = 2\mu\boldsymbol{\varepsilon} + \lambda \mathrm{tr}(\boldsymbol{\varepsilon})\mathbb{I},$$

where $\lambda = \lambda(\mathbf{x})$ and $\mu = \mu(\mathbf{x})$ are the Lamé elastic coefficients of the medium, $\mathrm{tr}(\cdot)$ is the trace operator and $\mathbb{I} \in \mathbb{R}^{m\times m}$ is the identity tensor. Here and in the following, we will suppose ρ, λ and μ to be uniformly bounded functions in Ω, i.e., $\rho, \lambda, \mu \in L^\infty(\Omega)$.
The semi-discretization of problem (35a)-(35e) by the DGSE technique [5] results into the following second order differential system for the nodal displacement $\mathbf{U}(t) = [\mathbf{U}^1(t), \mathbf{U}^2(t)]^T$

$$\begin{cases} M\ddot{\mathbf{U}}(t) + C\dot{\mathbf{U}}(t) + D\mathbf{U}(t) + A\mathbf{U}(t) = \mathbf{F}(t), \quad t \in (0, T], \\ \dot{\mathbf{U}}(0) = \mathbf{u}_1, \\ \mathbf{U}(0) = \mathbf{u}_0, \end{cases} \tag{36}$$

where $\ddot{\mathbf{U}}(t)$ (resp. $\dot{\mathbf{U}}(t)$) represents the vector of nodal acceleration (resp. velocity) and $\mathbf{F}(t)$ the vector of externally applied loads, i.e., $\mathbf{F}(t) = [\mathbf{F}^1(t), \mathbf{F}^2(t)]^T$ Here, M is the diagonal mass matrix, C and D stand for the structural damping (and have the same structure of M) while the action of the stiffness matrix A to the displacement vector $\mathbf{U}$ represents the internal (elastic) forces. We remark that the matrix A in (36) is symmetric and positive definite, see [5] for further details. The latter properties are also verified by the matrices M, C and D. In order to rewrite (36) in the form (1) we multiply it by $M^{-\frac{1}{2}}$ and set $\mathbf{Z}(t) = M^{\frac{1}{2}}\mathbf{U}(t)$ and obtain

$$\begin{cases} \ddot{\mathbf{Z}}(t) + L\dot{\mathbf{Z}}(t) + K\mathbf{Z}(t) = \mathbf{G}(t), \quad t \in (0, T], \\ \dot{\mathbf{Z}}(0) = M^{\frac{1}{2}}\mathbf{u}_1, \\ \mathbf{Z}(0) = M^{\frac{1}{2}}\mathbf{u}_0, \end{cases} \tag{37}$$

where $L = M^{-\frac{1}{2}}CM^{-\frac{1}{2}}$, $K = M^{-\frac{1}{2}}(D + A)M^{-\frac{1}{2}}$, are symmetric and positive definite and $\mathbf{G}(t) = M^{-\frac{1}{2}}\mathbf{F}(t)$.

5 Numerical results

In this section, we present some numerical results to highlight the behavior of the DG method presented in Section 2. In particular, we first focus our attention on a scalar benchmark, and later on we test it on the system of differential equations arisen by the space discretization of the elastodynamics problem.

5.1 Numerical results for a scalar problem

We consider the interval $I = (0, T]$, $T = 10$, subdivided into N time slab I_n, for $n = 1, ..., N$, of uniform length Δt. Moreover, we suppose the polynomial approximation vector $\mathbf{r}$ to be constant for each time slab, i.e., $r_1 = ... = r_N = r \geq 2$. We compute the error $|||u - u_{DG}|||$ versus $1/\Delta t$, with $\Delta t = 2^{-\ell}, \ell = 0, 1, 2, 3$, for several polynomial approximation degrees $r = 2, 3, 4, 5$. We consider the following problem

$$\begin{cases} \ddot{u}(t) + 5\dot{u}(t) + 6u(t) = 0, \qquad \forall t \in (0, 10], \\ u(0) = 2, \\ \dot{u}(0) = -5, \end{cases} \tag{38}$$

whose exact solution is $u(t) = e^{-3t} + e^{-2t}$, $t \in [0, 10]$.

The computed errors for the scalar test case are reported in Figure 2, in loglog scale. As expected a convergence rate of $\Delta t^{r-\frac{1}{2}}$ is observed (cf. Theorem 1). This is also confirmed by the results shown in Table 1, where the errors and the computed convergence rates are also reported. Although we do not have a theoretical proof, for completeness, we also report in Table 2 the computed error with respect to the $\|\cdot\|_{L^2(0,T)}$ and $\|\cdot\|_{H^1(0,T)}$ norms and the corresponding rates of convergence. The method achieves an optimal rate of convergence with respect to both norms, i.e., the error measured in the L^2-norm (resp. H^1-norm) decays as Δt^r (resp. Δt^{r-1}) for Δt going to 0. In Figure 3 we display the computed errors versus the polynomial degree for different values of Δt. As expected, an exponential convergence rate is observed.

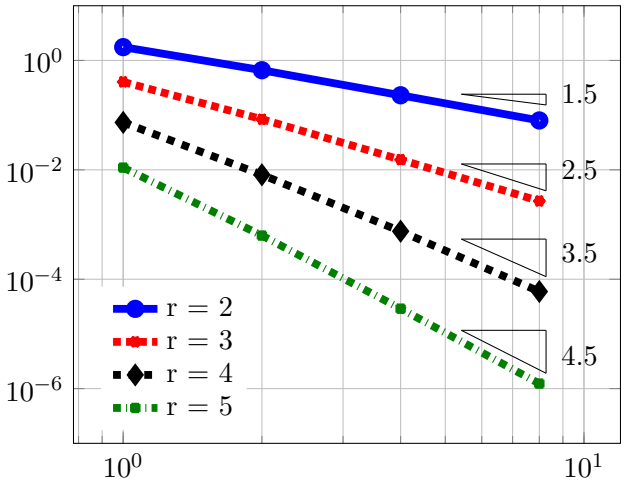

(a)

Figure 2: Scalar test case. Computed errors $|||u-u_{DG}|||$ versus $1/\Delta t$ for $\Delta t = 2^{-\ell}, \ell = 0, 1, 2, 3$ (left, loglog scale) and $r = 2, 3, 4, 5$.

Table 1: Scalar test case. Computed convergence rates in the $|||\cdot|||$ norm the with respect to the polynomial approximation degree $r = 2, 3, 4, 5$.

Δt	$r = 2$	$r = 3$	$r = 4$	$r = 5$
1.00e-0	-	-	-	-
5.00e-1	1.4017	2.2646	3.1802	4.1246
2.50e-1	1.5224	2.4577	3.4305	4.4403
1.25e-1	1.5295	2.5101	3.6584	4.5516

5.2 Numerical results for the elastodynamics problem

The numerical results presented in the sequel have been obtained by using the open source software SPEED (`http://speed.mox.polimi.it`) suitably adapted to apply the DG scheme presented in Section 2 to the system (37). For all the numerical simulations we consider the interval $I = (0, T]$ subdivided into N time slab I_n, for $n = 1, ..., N$ having uniform length Δt.

5.2.1 Test case 1

We consider $\Omega = (0, 1)^2, \Gamma_D = \partial\Omega$ and $T = 50$. We set the mass density $\rho = 1$, the Lamé coefficients $\lambda = \mu = 1$, $\zeta = 0.01$ and choose the data $\mathbf{f}, \mathbf{u}_0, \mathbf{u}_1$ such that the exact solution of problem in (35a)-(35e) is given by

$$\mathbf{u} = \sin(\sqrt{2}\pi t) \begin{bmatrix} -\sin^2(\pi x)\sin(2\pi y) \\ \sin(2\pi x)\sin^2(\pi y) \end{bmatrix}.$$

In the first example we compute the errors $|||\mathbf{u} - \mathbf{u}_{DG}|||$ versus $1/\Delta t$ for $\Delta t = 2^{-\ell}, \ell = 0, 1, 2, 3, 4$ and varying the polynomial degree $r = 2, 3, 4$. As of the space discretization of

Table 2: Scalar test case. Computed error in the $\|\cdot\|_{L^2(0,T)}$ and $\|\cdot\|_{H^1(0,T)}$ norms and corresponding convergence rates with respect to the polynomial approximation degree $r = 2, 3, 4, 5$.

r	Δt	$\|\cdot\|_{L^2(0,T)}$	rate	$\|\cdot\|_{H^1(0,T)}$	rate
2	1.00e-0	4.4902e-02	-	6.7961e-01	-
	8.00e-1	2.9612e-02	1.8655	4.9201e-01	1.4476
	4.00e-1	7.0288e-03	2.0749	1.5416e-01	1.6743
	2.00.e-1	1.2044e-03	2.5450	4.2254e-02	1.8672
	1.00.e-1	1.7331e-04	2.7968	1.0988e-02	1.9431
3	1.00e-0	6.9895e-03	-	1.4649e-01	-
	8.00e-1	3.9782e-03	2.5257	8.6484e-02	2.3617
	4.00e-1	4.5984e-04	3.1129	1.3821e-02	2.6455
	2.00.e-1	3.6876e-05	3.6404	1.8863e-03	2.8732
	1.00.e-1	2.5546e-06	3.8515	2.4343e-04	2.9540
4	1.00e-0	1.0209e-03	-	2.4885e-02	-
	8.00e-1	4.4989e-04	3.6723	1.1885e-02	3.3119
	4.00e-1	2.3662e-05	4.2489	9.6064e-04	3.6290
	2.00.e-1	9.0456e-07	4.7092	6.5449e-05	3.8755
	1.00.e-1	3.0658e-08	4.8829	4.2099e-06	3.9585
5	1.00e-0	1.2456e-04	-	3.4801e-03	-
	8.00e-1	4.2903e-05	4.7766	1.3399e-03	4.2773
	4.00e-1	1.0725e-06	5.3220	5.4621e-05	4.6165
	2.00.e-1	1.9994e-08	5.7452	1.8603e-06	4.8759
	1.00.e-1	3.3483e-10	5.9000	5.9740e-08	4.9607

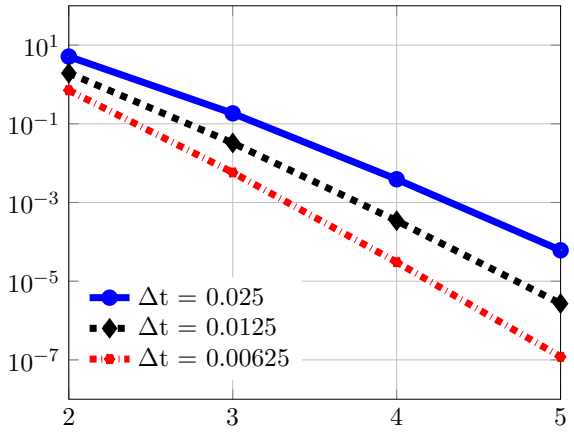

(a)

Figure 3: Scalar test case. Computed errors $|||u - u_{DG}|||$ versus $r = 2, 3, 4, 5$ (semilogy scale) for $\Delta t = 0.025, 0.0125, 0.00625$.

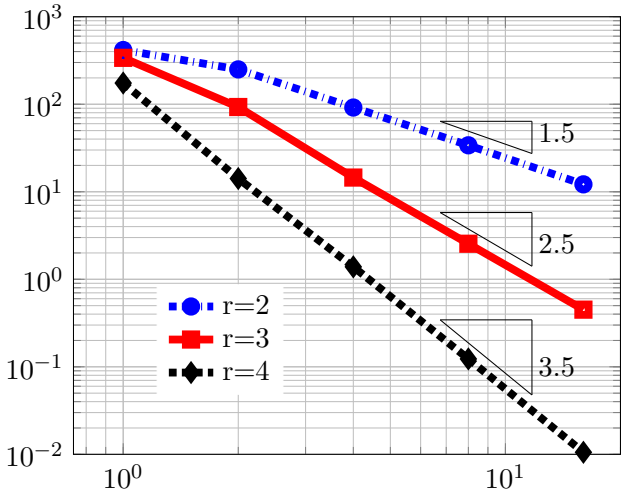

Figure 4: Test case 1. Computed errors $|||\mathbf{u} - \mathbf{u}_{DG}|||$ as a function of $1/\Delta t$ for $\Delta t = 2^{-\ell}, \ell = 0, 1, \ldots, 4$ (loglog scale), $r = 2, 3, 4$, $h = 0.125$ and $q = r + 1$.

the domain Ω we consider a Cartesian grid with characteristic size $h = 0.125$ and we set a polynomial approximation degrees $q = r + 1$. The computed errors are reported in Figure 4.

A convergence rate of $\Delta t^{r-\frac{1}{2}}$ is observed, in accordance with the theoretical estimate (32). In Table 3, the computed convergence rates are reported for $r = 2, 3, 4$, respectively.

5.2.2 Test case 2: a numerical test with non reflective boundary conditions

When simulating seismic wave propagations, ideally artificial boundaries should consent incident wave to be propagated without producing any reflection. A simple strategy consists in imposing non-reflective conditions on artificial boundaries $\Gamma_{NR} \subset \partial\Omega$ such that $\Gamma_{NR} \cap \Gamma_D \cap \Gamma_N = \emptyset$,

$$\begin{cases} \dfrac{\partial(\mathbf{u}\cdot\mathbf{n})}{\partial n} = -\dfrac{1}{V_P}\dfrac{\partial(\mathbf{u}\cdot\mathbf{n})}{\partial t} + \dfrac{V_S - V_P}{V_P}\dfrac{\partial(\mathbf{u}\cdot\boldsymbol{\tau})}{\partial t}, \\ \dfrac{\partial(\mathbf{u}\cdot\boldsymbol{\tau})}{\partial n} = -\dfrac{1}{V_S}\dfrac{\partial(\mathbf{u}\cdot\boldsymbol{\tau})}{\partial t} + \dfrac{V_S - V_P}{V_S}\dfrac{\partial(\mathbf{u}\cdot\mathbf{n})}{\partial t}, \end{cases} \tag{39}$$

where $\mathbf{n} = (n_1, n_2)$ (resp. $\boldsymbol{\tau} = (\tau_1, \tau_2)$) is the unit normal (resp. tangential) vector to $\partial\Omega$. Here, $V_P = \sqrt{(\lambda + 2\mu)/\rho}$ and $V_S = \sqrt{\mu/\rho}$ are the propagation velocities of compressional (P) and shear (S) waves, respectively. Equations (39) are first order non reflecting boundary conditions, see e.g., [42]. Their use yields a loss of symmetry in the matrix K in (37). The test consists of propagating a pure shear plane wave through a viscoelastic, horizontally layered soil profile, cf. Figure 5. The mechanical properties of the layers are summarized in Tab. 4. The incidence is orthogonal to the free surface and the excitation consists of a displacement Ricker wavelet $\mathbf{f}(\mathbf{x}, t) = h(t)\delta_q(\mathbf{x} - \mathbf{x}_0)$ with

$$h(t) = h_0(1 - 2(\pi f_{peak})^2(t - t_0)^2)e^{-(\pi f_{peak})^2(t-t_0)^2},$$

where $f_{peak} = 1\ Hz$, $t_0 = 2\ s$, and $h_0 = 1$ is the amplitude of the wave in time domain. Here δ_q is the numerical delta function, i.e. a polynomial of degree q that approximates the δ

Table 3: Test case 1. Computed errors $|||\mathbf{u} - \mathbf{u}_{DG}|||$ and computed convergence rates, $r = 2, 3, 4$, $h = 0.125$ and $q = r + 1$.

r	Δt	$\|\|\|\mathbf{u} - \mathbf{u}_{DG}\|\|\|$	rate
2	1.00e-0	4.1632e+02	-
	5.00e-1	2.5100e+02	0.7351
	2.50e-1	9.1706e+01	1.4474
	1.25e-1	3.3960e+01	1.4331
	6.25e-2	1.2156e+01	1.4821
3	1.00e-0	3.3909e+02	-
	5.00e-1	9.2986e+01	1.8665
	2.50e-1	1.4534e+01	2.6775
	1.25e-1	2.5484e+00	2.5117
	6.25e-2	4.4983e-01	2.5021
4	1.00e-0	1.7465e+02	-
	5.00e-1	1.4155e+01	3.6250
	2.50e-1	1.3873e+00	3.3509
	1.25e-1	1.2308e-01	3.4946
	6.25e-2	1.0550e-02	3.5441

Table 4: Mechanical properties

Material	ρ	λ	μ	ζ
1	2000	2.00e+07	2.00e+07	3.1416e-02
2	2000	5.00e+08	5.00e+08	3.1416e-03

distribution. In this case the forcing term is applied at points $\mathbf{x}_0$ lying at the bottom of the domain (see Figure 5).
The plane wave rises from the bottom of Ω, reaches the top of the computational domain, amplifying its amplitude (because of the free surface condition) and then is propagated backward, completely absorbed from the bottom boundary, thanks to the absorbing condition (39). To prevent spurious oscillations inside the domain, homogeneous Dirichlet boundary conditions (in y-direction) are imposed on the lateral sides of Ω, cf. Figure 5.

For the simulation we fix $T = 20\ s$, $\Delta t = 0.01\ s, h = 10$ and $q = 4$ for the space discretization while we use second order polynomials ($r = 2$) for the time integration. We compare the results obtained using the DG method with the analogous ones obtained coupling the DGSE space discretization with the classical leap-frog method [36] with $\Delta t = 0.0001\ s$. Notice that this is the biggest time step allowed by the CFL condition [15]. We plot the displacement time-histories (in the x-direction) recorded by two monitors: R_1 set on the free surface and R_2 located across Material 1 and Material 2 (cf. Figure 5). In Figure 6 we show the results obtained with the leap-frog and the DG method along with the semi-analytical solution $\mathbf{u}_{TH}$ based on the Thomson-Haskell propagation matrix method (see e.g. [23]). We can clearly see that all the methods produce almost identical solutions. To quantify the distance between the curves, in Figure 6 we plot the error $|\mathbf{u}_{TH}(t) - \mathbf{u}_*(t)|$ for $t \in (0, T]$,

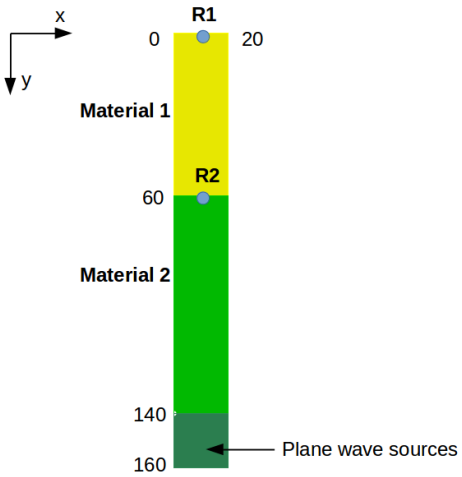

Figure 5: Domain Ω for the test case 2. Non reflective boundary conditions are imposed at the bottom edge, $\boldsymbol{\sigma}\mathbf{n} = \mathbf{0}$ is imposed at the top edge (free-surface condition), while homogeneous Dirichlet boundary conditions (in y-direction) are imposed on the lateral sides.

where $\mathbf{u}_*$ is either the solution obtained with the leap-frog scheme or the one obtained with the DG method and $\mathbf{u}_{TH}$ is the Thomson-Haskell semi-analytical solution. Both methods achieve the same level of accuracy.

6 Conclusions

In this work, we have developed a new high order Discontinuous Galerkin element method for the temporal discretization of second order ordinary Cauchy problems. To show the capabilities of our scheme we have applied it for the time integration of second order system of equations resulting after discontinuous spectral element semi-discretization (in space) of elastodynamics equation.
Our formulation contains suitable stabilization terms, which allowed the construction of an appropriate energy norm that naturally arose by the variational formulation of the problem. We have studied the well-posedness of the resulting scheme and proved *a priori* error estimates that properly depend on the local polynomial approximation degree and the local regularity of the exact solution. Our theoretical results have been confirmed by the numerical experiments carried out on both simplified test cases as well as on examples of practical interest.

Acknowledgements

Paola F. Antonietti and Ilario Mazzieri have been partially supported by the research grant no. 2015-0182 PolyNum: Polyhedral numerical methods for partial differential equations funded by Fondazione Cariplo and Regione Lombardia.

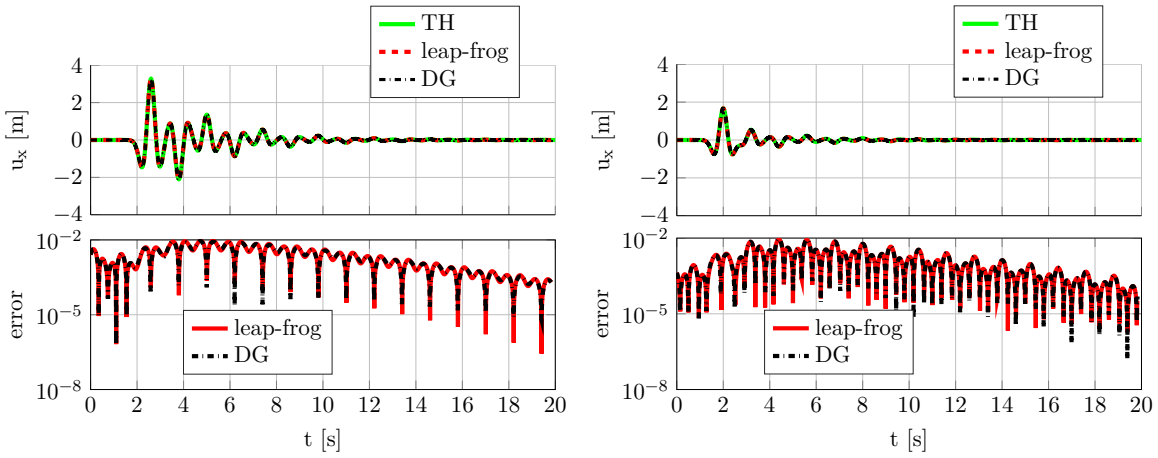

Figure 6: Displacement registered by R_1 (a) and R_2 (b).

References

[1] R. A. Adams and J. J. F. Fournier. *Sobolev spaces*, volume 140 of *Pure and Applied Mathematics*. Elsevier, Amsterdam, second edition, 2003.

[2] S. Adjerid and H. Temimi. A discontinuous Galerkin method for the wave equation. *Comput. Meth. Appl. Mech. Eng.*, 200(5–8):837 – 849, 2011.

[3] P. F. Antonietti, B. Ayuso de Dios, I. Mazzieri, and A. Quarteroni. Stability analysis of discontinuous Galerkin approximations to the elastodynamics problem. *J. Sci. Comput.*, pages 1–28, 2015.

[4] P. F. Antonietti, C. Marcati, I. Mazzieri, and A. Quarteroni. High order discontinuous Galerkin methods on simplicial elements for the elastodynamics equation. *Numer. Algorithms*, pages 1–26, 2015.

[5] P. F. Antonietti, I. Mazzieri, A. Quarteroni, and F. Rapetti. Non-conforming high order approximations of the elastodynamics equation. *Comput. Meth. Appl. Mech. Eng.*, 209212(0):212 – 238, 2012.

[6] D. N. Arnold. An interior penalty finite element method with discontinuous elements. *SIAM J. Numer. Anal.*, 19(4):742–760, 1982.

[7] D. N. Arnold, F. Brezzi, B. Cockburn, and L. D. Marini. Unified analysis of discontinuous Galerkin methods for elliptic problems. *SIAM J. Numer. Anal.*, 39(5):1749–1779, 2001-2002.

[8] I. Babuska and M. Suri. The $h - p$ version of the finite element method with quasiuniform meshes. *ESAIM: Mathematical Modelling and Numerical Analysis - Modélisation Mathématique et Analyse Numérique*, 21(2):199–238, 1987.

[9] M. Baccouch. A local discontinuous Galerkin method for the second-order wave equation. *Computer Methods in Applied Mechanics and Engineering*, 209212:129 – 143, 2012.

[10] H. T. Banks, M. J. Birch, M. P. Brewin, S. E. Greenwald, S. Hu, Z. R. Kenz, C. Kruse, M. Maischak, S. Shaw, and J. R. Whiteman. High-order space-time finite element schemes for acoustic and viscodynamic wave equations with temporal decoupling. *Int. J. Numer. Meth. Eng.*, 98(2):131–156, 2014.

[11] C. Bernardi and Y. Maday. *Theory and Numerics of Differential Equations: Durham 2000*, chapter Spectral, Spectral Element and Mortar Element Methods, pages 1–57. Springer Berlin Heidelberg, Berlin, Heidelberg, 2001.

[12] J. C. Butcher. *Numerical Methods for Ordinary Differential Equations*. John Wiley & Sons, Ltd, 2008.

[13] B. Cockburn and C.-W. Shu. The local discontinuous galerkin method for time-dependent convection-diffusion systems. *SIAM Journal on Numerical Analysis*, 35(6):2440–2463, 1998.

[14] F. Collino, T. Fouquet, and P. Joly. A conservative space-time mesh refinement method for the 1-d wave equation. Part I: Construction. *Numer. Math.*, 95(2):197–221, 2003.

[15] R. Courant, K. Friedrichs, and H. Lewy. Über die partiellen Differenzengleichungen der mathematischen Physik. *Math. Ann.*, 100(1):32–74, 1928.

[16] S. Delcourte and N. Glinsky. Analysis of a high-order space and time discontinuous Galerkin method for elastodynamic equations. application to 3d wave propagation. *ESAIM: M2AN*, 49(4):1085–1126, 2015.

[17] M. Delfour, W. Hager, and F. Trochu. Discontinuous Galerkin methods for ordinary differential equations. *Mathematics of Computation*, 36(154):455–473, 1981.

[18] D. A. Di Pietro and A. Ern. *Mathematical Aspects of Discontinuous Galerkin Methods*, volume 69 of *Mathématiques et Applications*. Springer, Berlin, 2012.

[19] J. Diaz and M. J. Grote. Energy conserving explicit local time stepping for second-order wave equations. *SIAM J. Sci. Comput.*, 31(3):1985–2014, 2009.

[20] M. Dumbser, M. Käser, and E. Toro. An arbitrary high-order Discontinuous Galerkin method for elastic waves on unstructured meshes - V. Local time stepping and p-adaptivity. *Geophys. J. Int.*, 171(2):695–717, 2007.

[21] M. J. Grote and T. Mitkova. High-order explicit local time-stepping methods for damped wave equations. *J. Comput. Appl. Math.*, 239(0):270 – 289, 2013.

[22] M. J. Grote, A. Schneebeli, and D. Schötzau. Discontinuous Galerkin finite element method for the wave equation. *SIAM J. Numer. Anal.*, 44(6):2408–2431, 2006.

[23] N. A. Haskell. The dispersion of surface waves on multilayered media. *Bull. Seismol. Soc. Am.*, 43:17–43, 1953.

[24] J. Hesthaven and T. Warburton. *Nodal discontinuous Galerkin methods*, volume 54 of *Texts in Applied Mathematics*. Springer, Berlin, 2008.

[25] P. Houston, C. Schwab, and E. Süli. Stabilized hp-finite element methods for first-order hyperbolic problems. *SIAM Journal on Numerical Analysis*, 37(5):1618–1643, 2000.

[26] T. J. Hughes and G. M. Hulbert. Space-time finite element methods for elastodynamics: formulations and error estimates. *Comput. Meth. Appl. Mech. Eng.*, 66(3):339–363, 1988.

[27] T. J. Hughes and J. R. Stewart. A space-time formulation for multiscale phenomena. *Journal of Computational and Applied Mathematics*, 74(1-2):217 – 229, 1996.

[28] G. M. Hulbert and T. J. Hughes. Space-time finite element methods for second-order hyperbolic equations. *Comput. Meth. Appl. Mech. Eng.*, 84(3):327–348, 1990.

[29] C. Johnson. Discontinuous Galerkin finite element methods for second order hyperbolic problems. *Comput. Meth. Appl. Mech. Eng.*, 107(1):117–129, 1993.

[30] A. Kroopnick. Bounded and l^2-solutions to a second order nonlinear differential equation with a square integrable forcing term. *Internat. J. Math. Math. Sci.*, 22(3):569–571, 1999.

[31] R. Le Veque. *Finite Difference Methods for Ordinary and Partial Differential Equations.* SIAM - Society for Industrial and Applied Mathematics, 2007.

[32] P. Lesaint and P. Raviart. *On a Finite Element Method for Solving the Neutron Transport Equation.* Univ. Paris VI, Labo. Analyse Numérique, 1974.

[33] I. Mazzieri, M. Stupazzini, R. Guidotti, and C. Smerzini. Speed: Spectral elements in elastodynamics with discontinuous Galerkin: a non-conforming approach for 3d multi-scale problems. *Int. J. Numer. Meth. Eng.*, 95(12):991–1010, 2013.

[34] A. Quarteroni. *Numerical models for differential problems*, volume 8 of *MS&A. Modeling, Simulation and Applications.* Springer-Verlag Italia, Milan, 2014.

[35] A. Quarteroni, R. Sacco, and F. Saleri. *Numerical mathematics*, volume 37 of *Texts in Applied Mathematics.* Springer-Verlag, Berlin, second edition, 2007.

[36] A. Quarteroni and A. Valli. *Numerical Approximation of Partial Differential Equations.* Springer Series in Computational Mathematics. Springer, 2008.

[37] W. H. Reed and T. R. Hill. Triangular mesh methods for the neutron transport equation. Technical Report LA-UR-73-479, Los Alamos Scientific Laboratory, 1973.

[38] B. Rivière. *Discontinuous Galerkin Methods for Solving Elliptic and Parabolic Equations.* Society for Industrial and Applied Mathematics, 2008.

[39] B. Rivière and M. F. Wheeler. Discontinuous finite element methods for acoustic and elastic wave problems. In *Current trends in scientific computing (Xi'an, 2002)*, volume 329 of *Contemp. Math.*, pages 271–282. Amer. Math. Soc., Providence, RI, 2003.

[40] D. Schötzau and C. Schwab. Time discretization of parabolic problems by the hp-version of the discontinuous Galerkin finite element method. *SIAM Journal on Numerical Analysis*, 38(3):837–875, 2000.

[41] C. Schwab. *p- and hp- Finite Element Methods. Theory and Applications in Solid and Fluid Mechanics.* Oxford University Press, New York, United States, 1998.

[42] R. Stacey. Improved transparent boundary formulations for the elastic-wave equation. *Bull. Seismol. Soc. Am.*, 78(6):2089–2097, 1988.

[43] A. Taube, M. Dumbser, C.-D. Munz, and R. Schneider. A high-order discontinuous Galerkin method with time-accurate local time stepping for the Maxwell equations. *Int. J. Numer. Model. El.*, 22(1):77–103, 2009.

[44] L. L. Thompson and P. M. Pinsky. A space-time finite element method for structural acoustics in infinite domains part 1: Formulation, stability and convergence. *Comput. Meth. Appl. Mech. Eng.*, 132(3):195–227, 1996.

[45] J. van der Vegt, C. Klaij, F. van der Bos, and H. van der Ven. Space-time discontinuous Galerkin method for the compressible Navier-Stokes equations on deforming meshes. In P. Wesseling, E. Onate, and J. Periaux, editors, *European Conference on Computational Fluid Dynamics ECCOMAS CFD 2006*, Delft, 2006. TU Delft.

[46] N. J. Walkington. Combined dg–cg time stepping for wave equations. *SIAM J. Numer. Anal.*, 52(3):1398–1417, 2014.

[47] T. Werder, K. Gerdes, D. Schötzau, and C. Schwab. hp-discontinuous Galerkin time stepping for parabolic problems. *Comput. Meth. Appl. Mech. Eng.*, 190(4950):6685 – 6708, 2001.

[48] M. F. Wheeler. An elliptic collocation-finite element method with interior penalties. *SIAM Journal on Numerical Analysis*, 15(1):152–161, 1978.

[49] L. C. Wilcox, G. Stadler, C. Burstedde, and O. Ghattas. A high-order discontinuous Galerkin method for wave propagation through coupled elastic-acoustic media. *J. Comput. Phys.*, 229(24):9373 – 9396, 2010.

[50] Y. Yang, S. Chirputkar, D. N. Alpert, T. Eason, S. Spottswood, and D. Qian. Enriched spacetime finite element method: a new paradigm for multiscaling from elastodynamics to molecular dynamics. *Int. J. Numer. Meth. Eng.*, 92(2):115–140, 2012.

Appendix

In this appendix we collect some technical results used for the proofs of Lemmas 3.1 and 3.2.

Calculation of expansion coefficients (13)–(15).

Proof. We start by writing the projection operator Π^r as

$$\Pi^r u = \sum_{i=1}^{r-3} u_i L_i + u^*_{r-2} L_{r-2} + u^*_{r-1} L_{r-1} + u^*_r L_r,$$

being L_i, $i \geq 0$, the Legendre polynomial of degree i in $\mathbb{P}^i(I)$, with $I = (-1, 1)$. Due to the orthogonality of the Legendre polynomials, (11d) is easily verified. Then, we determine the unknown coefficients u^*_{r-2}, u^*_{r-1} and u^*_r by imposing conditions (11a)–(11c). In particular, we have that

$$\text{(11a)} \implies u^*_{r-2} + u^*_{r-1} + u^*_r = \sum_{i=r-2}^{\infty} u_i, \tag{40}$$

$$\text{(11b)} \implies u^*_{r-2} - u^*_{r-1} + u^*_r = (-1)^r \sum_{i=r-2}^{\infty} (-1)^i u_i, \tag{41}$$

$$\text{(11c)} \implies \frac{(r-2)(r-1)}{2} u^*_{r-2} + \frac{(r-1)r}{2} u^*_{r-1} + \frac{r(r+1)}{2} u^*_r = \sum_{i=r-2}^{\infty} \frac{i(i+1)}{2} u_i. \tag{42}$$

By adding (40) to (41) we obtain the expression of u^*_{r-1} as

$$u^*_{r-1} = \frac{1}{2} \sum_{i=r-2}^{\infty} u_i - \frac{1}{2} \sum_{i=r-2}^{\infty} (-1)^{r+i} u_i. \tag{43}$$

Next, using (43) into (40) we obtain

$$u^*_{r-2} = \frac{1}{2} \sum_{i=r-2}^{\infty} u_i + \frac{1}{2} \sum_{i=r-2}^{\infty} (-1)^{r+i} u_i - u^*_r. \tag{44}$$

Substituting (43) and (44) into (42) we can write

$$u^*_r = \frac{1}{(2r-1)} \sum_{i=r-2}^{\infty} \frac{i(i+1)}{2} u_i - \frac{(r-1)^2}{2(2r-1)} \sum_{i=r-2}^{\infty} u_i + \frac{(r-1)}{2(2r-1)} \sum_{i=r-2}^{\infty} (-1)^{r+i} u_i \tag{45}$$

and consequently we can determine the expression of u^*_{r-2} as

$$u^*_{r-2} = -\frac{1}{(2r-1)} \sum_{i=r-2}^{\infty} \frac{i(i+1)}{2} u_i + \frac{r^2}{2(2r-1)} \sum_{i=r-2}^{\infty} u_i + \frac{r}{2(2r-1)} \sum_{i=r-2}^{\infty} (-1)^{r+i} u_i. \tag{46}$$

Finally, it is easy to verify that

$$u_{r-2} = -\frac{1}{(2r-1)}\sum_{i=r-2}^{r}\frac{i(i+1)}{2}u_i + \frac{r^2}{2(2r-1)}\sum_{i=r-2}^{r}u_i + \frac{r}{2(2r-1)}\sum_{i=r-2}^{r}(-1)^{r+i}u_i$$
$$u_{r-1} = \frac{1}{2}\sum_{i=r-2}^{r}u_i - \frac{1}{2}\sum_{i=r-2}^{r}(-1)^{r+i}u_i$$
$$u_r = \frac{1}{(2r-1)}\sum_{i=r-2}^{r}\frac{i(i+1)}{2}u_i - \frac{(r-1)^2}{2(2r-1)}\sum_{i=r-2}^{r}u_i + \frac{(r-1)}{2(2r-1)}\sum_{i=r-2}^{r}(-1)^{r+i}u_i.$$

□

Proof of equation (17).

Proof. First of all we notice that for $i \geq 2$ we have

$$\begin{aligned} u_i &= \frac{b_{i-1}}{2i-1} - \frac{b_{i+1}}{2i+3} \\ &= \frac{1}{2i+1}\left(\frac{c_{i-2}}{2i-3} - \frac{c_i}{2i+1}\right) - \frac{1}{2i+3}\left(\frac{c_i}{2i+1} - \frac{c_{i+2}}{2i+5}\right) \\ &= \frac{c_{i-2}}{(2i-1)(2i-3)} - \frac{2c_i}{(2i-1)(2i+3)} + \frac{c_{i+2}}{(2i+3)(2i+5)}. \end{aligned}$$

Then, it follows that

$$\begin{aligned} \sum_{i=r+1}^{\infty} i(i+1)u_i &= \sum_{i=r+1}^{\infty}\frac{i(i+1)c_{i-2}}{(2i-1)(2i-3)} - \sum_{i=r+1}^{\infty}\frac{2i(i+1)c_i}{(2i-1)(2i+3)} + \sum_{i=r+1}^{\infty}\frac{i(i+1)c_{i+2}}{(2i+3)(2i+5)} \\ &= \sum_{i=r-1}^{\infty}\frac{(i+2)(i+3)c_i}{(2i+3)(2i+1)} - \sum_{i=r+1}^{\infty}\frac{2i(i+1)c_i}{(2i-1)(2i+3)} + \sum_{i=r+3}^{\infty}\frac{(i-2)(i-1)c_i}{(2i-1)(2i+1)} \\ &= \sum_{i=r-1}^{r+2}\frac{(i+2)(i+3)c_i}{(2i+3)(2i+1)} - \sum_{i=r+1}^{r+2}\frac{2i(i+1)c_i}{(2i-1)(2i+3)} \\ &= \sum_{i=r-1}^{r}\frac{(i+2)(i+3)c_i}{(2i+3)(2i+1)} + \sum_{i=r+1}^{r+2}\left(\frac{(i+2)(i+3)c_i}{(2i+1)(2i+3)} - \frac{2i(i+1)c_i}{(2i-1)(2i+3)}\right) \\ &= \sum_{i=r-1}^{r}\frac{(i+2)(i+3)c_i}{(2i+3)(2i+1)} - \sum_{i=r+1}^{r+2}\frac{(i-1)(i-2)c_i}{(2i+1)(2i-1)} \\ &= \frac{(r+1)(r+2)}{(2r-1)(2r+1)}c_{r-1} + \frac{(r+2)(r+3)}{(2r+1)(2r+3)}c_r \\ &\qquad - \frac{r(r-1)}{(2r+1)(2r+3)}c_{r+1} - \frac{r(r+1)}{(2r+3)(2r+5)}c_{r+2}. \end{aligned}$$

□

MOX Technical Reports, last issues

Dipartimento di Matematica
Politecnico di Milano, Via Bonardi 9 - 20133 Milano (Italy)

26/2016 Brunetto, D.; Calderoni, F.; Piccardi, C.
Communities in criminal networks: A case study

27/2016 Repossi, E.; Rosso, R.; Verani, M.
A phase-field model for liquid-gas mixtures: mathematical modelling and Discontinuous Galerkin discretization

25/2016 Baroli, D.; Cova, C.M.; Perotto, S.; Sala, L.; Veneziani, A.
Hi-POD solution of parametrized fluid dynamics problems: preliminary results

24/2016 Pagani, S.; Manzoni, A.; Quarteroni, A.
A Reduced Basis Ensemble Kalman Filter for State/parameter Identification in Large-scale Nonlinear Dynamical Systems

23/2016 Fedele, M.; Faggiano, E.; Dedè, L.; Quarteroni, A.
A Patient-Specific Aortic Valve Model based on Moving Resistive Immersed Implicit Surfaces

22/2016 Antonietti, P.F.; Facciola', C.; Russo, A.;Verani, M.
Discontinuous Galerkin approximation of flows in fractured porous media

21/2016 Ambrosi, D.; Zanzottera, A.
Mechanics and polarity in cell motility

19/2016 Guerciotti, B.; Vergara, C.
Computational comparison between Newtonian and non-Newtonian blood rheologies in stenotic vessels

20/2016 Wilhelm, M.; Sangalli, L.M.
Generalized Spatial Regression with Differential Regularization

Guerciotti, B.; Vergara, C.
Computational comparison between Newtonian and non-Newtonian blood rheologies in stenotic vessels